Penukula *et al. Energy Mater* 2024;4:400060
DOI: 10.20517/energymater.2024.26

Energy Materials

Article

Open Access

Check for updates

Use of carbon electrodes to reduce mobile ion concentration and improve reliability of metal halide perovskite photovoltaics

Saivineeth Penukula[1], Favian Tippin[1], Muzhi Li[1], Kausar Ali Khawaja[2], Feng Yan[2], Nicholas Rolston[1,*]

[1]Renewable Energy Materials and Devices Lab, School of Electrical, Computer and Energy Engineering (ECEE), Arizona State University, Tempe, AZ 85284, USA.
[2]School for Engineering of Matter, Transport and Energy, Arizona State University, Tempe, AZ 85281, USA.

***Correspondence to:** Prof. Nicholas Rolston, Renewable Energy Materials and Devices Lab, School of Electrical, Computer and Energy Engineering (ECEE), Arizona State University, 7700 S River Pkwy, Tempe, AZ 85284, USA. E-mail: nicholas.rolston@asu.edu

How to cite this article: Penukula S, Tippin F, Li M, Khawaja KA, Yan F, Rolston N. Use of carbon electrodes to reduce mobile ion concentration and improve reliability of metal halide perovskite photovoltaics. *Energy Mater* 2024;4:400060. https://dx.doi.org/10.20517/energymater.2024.26

Received: 2 Apr 2024 **First Decision:** 22 Apr 2024 **Revised:** 1 May 2024 **Accepted:** 16 May 2024 **Published:** 7 Jun 2024

Academic Editor: Ahmad Amiri **Copy Editor:** Fangling Lan **Production Editor:** Fangling Lan

Abstract

Ion migration is one of the prime reasons for the rapid degradation of metal halide perovskite solar cells (PSCs), and we report on a method for quantifying mobile ion concentration (N_o) using a transient dark current measurement. We perform both *ex-situ* and *in-situ* measurements on PSCs and study the evolution of N_o in films and devices under a range of temperatures. We also study the effect of device architecture, top electrode chemistry, and metal halide perovskite composition and dimensionality on N_o. Two-dimensional perovskites are shown to reduce the ion concentration along with inert C electrodes that do not react with halides by ~99% while also improving mechanical reliability by ~250%. We believe this work can provide design guidelines for the development of stable PSCs through the lens of minimizing mobile ions and their evolution over time under operational conditions.

Keywords: Perovskite solar cells, ion migration, 2D perovskite, stability, transient dark current, electrochemistry

© The Author(s) 2024. **Open Access** This article is licensed under a Creative Commons Attribution 4.0 International License (https://creativecommons.org/licenses/by/4.0/), which permits unrestricted use, sharing, adaptation, distribution and reproduction in any medium or format, for any purpose, even commercially, as long as you give appropriate credit to the original author(s) and the source, provide a link to the Creative Commons license, and indicate if changes were made.

INTRODUCTION

Currently, commercialized solar panels operate at approximately 21% efficiency with top consumer brands boasting ~24.9% efficiency[1]. However, the manufacturing process for consumer solar panels is expensive with limited efficiency improvements possible for incumbent technology[2]. To combat this, researchers are investigating alternative solar technologies including different photovoltaic semiconductor materials such as metal halide-based perovskite solar cells (PSCs). PSCs offer promising prospects due to their cost-effectiveness and near-comparable efficiency to traditional silicon-based cells[3] with the current highest efficiency being 26.1%[4]. The main reason for their lack of widespread use in industry is their limited lifespan. PSCs in their current form degrade more quickly to replace silicon-based solar cells at the consumer level but there is ongoing research into the underlying mechanisms that cause this degradation including ion migration[5-7].

Ion migration is a phenomenon that happens in metal halide perovskites (MHPs) because of the soft crystal lattice of the material leading to the formation of ionic defects (such as vacancies and interstitials) that act as mobile ions in the lattice[8,9]. The primary mechanism for this is through halide vacancies that exhibit low activation energies in the MHP lattice both intrinsically and under the influence of external stimuli such as heat and light. The consequences of ion migration are phase separation and electrochemical reactions with transport layers and electrodes, affecting their extraction properties that induce material degradation and electronic losses[7,10-13]. It has been shown in our previous work that ion migration in PSCs and MHPs can be quantified in terms of a mobile ion concentration (N_o)[6].

Compositional changes to the structure of the perovskite such as two-dimensional (2D) MHPs where the A-site cations of the MHP are replaced by larger organic cations leading to the formation of a layered structure with increased bandgaps are more stable than their three-dimensional (3D) counterparts[14-16]. Part of this effect is due to the reduced volatility and hydrophobicity of the bulky 2D cations that can improve the operational stability of PSCs in terms of chemical, thermal, and environmental stability[17,18]. To enable improved stability without reducing the performance of PSCs, 2D/3D heterostructures are commonly used[19].

Metal top electrodes in PSCs, particularly silver (Ag), are prone to irreversible corrosion due to ion migration by the reaction of metal with the halide components in the MHP, leading to PSC performance losses[20-22]. It has also been shown that metal ions can diffuse into the MHP and cause irreversible degradation[23,24]. Alternative metal electrodes, such as copper (Cu), gold (Au), and aluminum (Al), are also known to form metal-halide complexes with the MHP and are also prone to oxidation in the presence of oxygen and moisture that degrade PSC performance[25,26]. Carbon (C) electrodes in place of their metal counterparts are shown to be more stable thermally and chemically and are less prone to oxidation and corrosion[20,27,28]. PSCs utilizing C electrodes offer a promising solution due to their potential for extended durability and cost-effectiveness. Various C-based materials have been used, including pure carbon ink, graphite, carbon nanotubes, and graphene[29-33]. C-based materials safeguard the perovskite layer from both moisture and heat-induced degradation, thereby enhancing the long-term stability of these solar cells[34,35]. However, the performance of PSCs utilizing C electrodes typically lags behind that of those employing metal electrodes. This is primarily attributed to the elevated resistivity of C materials and the relatively lower quality of the C/hole-transport layer (HTL) interface compared to the metal/HTL interface. Although C-based materials are generally more economical than noble metals, the large-scale industrial production of high-performance C-based PSCs continues to be a challenge[36,37]. In this work, we selected a low-cost, commercially available C-based ink as the top electrode for PSCs to quantify the impact that C electrodes have on the ionic and thermomechanical stability of PSCs.

In this work, we demonstrate how a transient dark current response is used to extract N_o from MHP thin films or PSCs, and how N_o can serve as a metric to determine the onset of degradation in MHP thin films based on its evolution with aging. Compositional effects of N_o such as dependence on the dimensionality of the MHP and compositional tuning are demonstrated. We also report on using C electrodes in place of Ag electrodes to reduce N_o in the PSCs over a wide range of temperatures and with aging along with an increase in the mechanical robustness.

EXPERIMENTAL

The substrate preparation steps before depositing the perovskite precursors or any of the transport layers are as follows: Indium tin oxide coated glass (ITO-glass) substrates (Xin Yan Technologies) are initially cleaned with an industry-grade soap solution of Extran mixed with water in the ratio of 1:10 for 10 min in an ultrasonic cleaner. After that, the ITO-glass slides are cleaned with de-ionized water, and the surface of the slides is cleaned with a brush to remove the residual soap. The glass slides are then cleaned with isopropyl alcohol (IPA) and acetone (Alfa Aesar - 99.5%+) separately for 10 min and then subjected to ultraviolet and ozone treatment for 10 min.

Cesium formamidinium lead iodide ($Cs_{0.2}FA_{0.8}PbI_3$)

The perovskite precursor solution for $Cs_{0.2}FA_{0.8}PbI_3$ films is prepared by mixing 0.2% Cesium Iodide (CsI) (Sigma-Aldrich - 99.999% trace metals basis), 0.8% Formamidinium Iodide (FAI) (Greatcell Solar Materials), and Lead Iodide (PbI_2) (TCI America - 99.99% trace metals basis). A measure of 1 mL, 1 M concentration solution is made by mixing 0.0519 gm of CsI, 0.1375 gm of FAI, and 0.461 gm of PbI_2 in a solvent of 4:1 Dimethylformamide (DMF) (Sigma-Aldrich - Anhydrous 99.8%) and Dimethyl Sulfoxide (DMSO) (Sigma-Aldrich - Anhydrous ≥ 99.9%) with 800 µL of DMF and 200 µL of DMSO. A vortex mixer is used to mix the solution until a clear solution is formed. $Cs_{0.2}FA_{0.8}PbI_3$ films on ITO-glass were fabricated using spin coating. A two-step spin coating process with anti-solvent quenching was used where a measure of 100 µL of perovskite precursor was deposited on the glass substrate and spun at a speed of 1,000 rpm and acceleration of 500 rpm/s for 10 s and then the speed was stepped up to 5,000 rpm and acceleration of 1,500 rpm/s for 10 s. A measure of 100 µL of chlorobenzene (anti-solvent) (Sigma-Aldrich - Anhydrous 99.8%) was dropped on the sample at the last 3-5 s of the second step, and then the samples were annealed at 150 °C for 10 min.

Methylammonium lead iodide ($MAPbI_3$)

The precursor solution for methylammonium lead iodide ($MAPbI_3$) is prepared by mixing methylammonium iodide (MAI) (Greatcell Solar Materials) and PbI_2. A measure of 1 mL, 1 M concentration solution is made by mixing 0.159 gm of MAI and 0.461 gm of PbI_2 in a solvent of 4:1 DMF to DMSO with 800 µL DMF and 200 µL DMSO, and the solution is mixed in a vortex mixer until a clear solution is formed. $MAPbI_3$ films on ITO-glass were fabricated following the same procedure showcased in previous work[6].

Ruddlesden popper 2D perovskite

The precursor solution for [Ruddlesden Popper (RP), with butylammonium] phase $n = 1$ $[(BA)_2PbI_4]$ 2D perovskite is prepared by mixing butylammonium iodide (BAI) (Greatcell Solar Materials) and PbI_2. A measure of 1 mL, 1 M concentration solution is made by mixing 0.201 gm of BAI and 0.461 gm of PbI_2 in a solvent of 2:3 DMF to DMSO with 0.4 mL DMF and 0.6 mL DMSO. A 4 wt% polyvinylpyrrolidone (PVP with 10,000 average molecular weight) (Sigma-Aldrich) is then added to the solution and mixed in a vortex mixer until a clear solution is formed. A similar process is used to make RP phase $n = 2$ $[(BA)_2(MA)Pb_2I_7]$ 2D perovskite by mixing 0.201 gm of BAI, 0.0795 gm of MAI, and 0.461 gm of PbI_2.

Dion-jacobson 2D perovskite

The precursor solution for [Dion-Jacobson (DJ), with propane-1,3-diammonium] phase n = 1 2D perovskite is prepared by mixing propane-1,3-diammonium iodide ($PDAI_2$) (Greatcell Solar Materials) and PbI_2. A measure of 1 mL, 1 M concentration solution is made by mixing 0.3295 gm of $PDAI_2$ and 0.461 gm of PbI_2 in a solvent of 2:3 DMF to DMSO with 0.4 mL DMF and 0.6 mL DMSO. A 4 wt% PVP (with 10,000 average molecular weight) is then added to the solution and mixed in a vortex mixer until a clear solution is formed. A similar process is used to make DJ phase n = 4 [$PDA(MA)_3Pb_4I_{13}$] 2D perovskite by mixing 0.0824 gm of $PDAI_2$, 0.119 gm of MAI, and 0.461 gm of PbI_2.

Using spin coating, 2D MHP thin films (both RP and DJ phases) on ITO-glass were fabricated. A single-step spin coating process was used where 200 µL of perovskite ink was deposited on the substrate and spun at a speed of 2,000 rpm and acceleration of 500 rpm/s for 30 s and annealed at 100 °C for 10 min.

Cesium lead iodide ($CsPbI_3$)

The precursor solution for $CsPbI_3$ films is made by mixing CsI and PbI_2 following the recipe in the literature[38]. A measure of 1 mL, 0.8 M concentration solution was made by mixing 0.2076 gm of CsI and 0.3688 gm of PbI_2 in a solvent of 1:4 DMF and DMSO with 200 µL DMF and 800 µL DMSO. A 3 wt% PVP is then added to the solution and mixed in a vortex mixer until a clear solution is formed. $CsPbI_3$ films on ITO-glass were fabricated following the same procedure showcased in previous work[38].

Double halide perovskite ($Cs_{0.05}FA_{0.85}MA_{0.1}PbI_{2.55}Br_{0.45}$)

The solution for the $Cs_{0.05}FA_{0.81}MA_{0.14}PbI_{2.55}Br_{0.45}$ precursor was prepared using molar ratios of PbI_2 (1.1 M), $PbBr_2$ (0.2 M), FAI (1 M), MABr (0.2 M), and CsI (1.5 M dissolved in DMSO). These compounds were dissolved in a mixed solvent of DMF and DMSO, with a volume ratio of 4:1. Subsequently, the prepared perovskite precursor underwent stirring at 70 °C for 4 h.

Nickel-oxide (NiO_x)

NiO_x solution for depositing the hole transport layer (HTL) is prepared by mixing 1 M $NiNO_3$. $(H_2O)_6$ (99.999% trace metals basis) in 94% ethylene glycol (EG) (thermo scientific - anhydrous 99.8%) and 6% ethylenediamine (EDA) (Thermo scientific - 99%); the vial is then placed in a vortex mixer, and the solution is mixed until it turns into a dark blue color indicating the solubility of the precursor into the solvent.

Perovskite solar cells (PSCs)

PSCs with the composition of $MAPbI_3$ with a device structure of Glass/ITO/NiO_x/perovskite/C_{60}/Ag and with the composition of $(Cs_{0.25}FA_{0.75})Pb(I_{0.8}Br_{0.2})_3$ + 4 mol% $MAPbCl_3$[39] with a device structure of Glass/ITO/poly-TPD/PFN/perovskite/C_{60}/Ag were fabricated in a p-i-n format following the same procedure showcased in the previous work[6]. After the substrate preparation, the PSCs are fabricated in a step-by-step procedure where HTL and the perovskite absorber layers are deposited using spin coating, and the electron transport layer (ETL) and Ag top contact are deposited using evaporation in that order. A C top electrode is formed on the PSC by depositing it from the solvent-based C paste (solvent C) which is a mixture of graphite and carbon black (PELCO conductive carbon glue - Ted Pella).

PSCs with the composition of $Cs_{0.05}FA_{0.81}MA_{0.14}PbI_{2.55}Br_{0.45}$ with a device structure of Glass/ITO/SnO_2/perovskite/2D MHP/solvent-free C were fabricated in an n-i-p format following the procedure showcased in the previous work[40]. A 2D MHP precursor was made by making a solution containing 2.5 mg of phenethylammonium iodide (PEAI) dissolved in 1 mL of IPA. Additionally, 60 mL of this 2D solution was spin-coated onto the perovskite film at 3,000 rpm for 30 s. A 75 mm free-standing carbon film was created

using a solvent exchange technique[41]. The electrode was then hot-pressed onto the 2D MHP layer at 100 psi and 80 °C for 1 min[40].

Characterization

All the ionic and electronic measurements were performed with PAIOS, an all-in-one measurement equipment for photovoltaic devices and light-emitting diodes (LEDs). *In-situ* ionic measurements were performed with the temperature control stage and module (LTS-420E) from Linkam in integration with PAIOS. The LTS-420E provided higher temperatures to the samples (from -195 to 420 °C with integrated electrical probes). A flow of liquid nitrogen (LN_2) through the stage was used for cooling. A heating pad was used to age the MHP thin films and PSCs (aged as is) at 45 or 65 °C in a N_2 glovebox for the period they were aged with *ex-situ* measurements on PAIOS at 24 h intervals. The aging process followed for MHP thin films involved aging a layer stack of ITO-Glass/MHP and then adding the electrode on the sample after aging while making the measurements; this was done to avoid any involvement from the solvents present in the C paste used for the electrode during aging. N_o was measured and calculated using the transient dark current method as described in our previous work[6] in which a voltage bias of 800 mV is applied to the PSC in the forwards-bias configuration in the form of a pulse with the following characteristics: 1 ms settling time, 10 ms pulse time, 1 ms follow-up time. The entire measurement lasts around 13 ms with the measurement cut-off around 1 ms after the bias is taken away which gives the mobile ions in the PSC enough time to fully drift. The measured drift current can be time-integrated and divided by the elementary charge, area, and thickness of the MHP layer, respectively, to determine N_o.

Fracture energy (G_c) was measured with a standard fracture specimen configuration called a double cantilever beam (DCB). To create a DCB fracture sample, a layer of thin epoxy was applied to cover glass with the identical dimensions as the substrate glass for the device/stack and then bonded to the device/stack to create a sandwich-like structure with the device layers bonded between glass at room temperature. G_c was then calculated and averaged based on the method showcased elsewhere[42].

RESULTS AND DISCUSSION

We first conducted *ex-situ* N_o and current-voltage (I-V) measurements on $MAPbI_3$ films with the layer stack of ITO-Glass/MHP/solvent C before and after exposure to 85 °C for a total of 96 h following the aforementioned aging procedure of the MHP thin films in a N_2 glove box to prevent moisture-induced degradation. The results of the I-V response and transient dark current shown in Figure 1A and B were obtained before any exposure. From the I-V curve, the film operated normally with around a 1.1 V turn-on voltage and a N_o value of 1.55×10^{12} cm^{-3} before exposure. However, after heat exposure, as shown in Figure 1C and D, there was no ionic (drift current) response due to the resistor-like behavior of the degraded MHP generating a current at the applied bias of 0.8 V. Since the N_o measurement comes from integrating the drift current response, there was no possible way to extract N_o after exposure. Supplementary Figure 1 shows images of the MHP throughout the heat exposure revealing noticeable visual changes as the film degraded.

To study the effect of mobile ion changes in a more thermally stable MHP absorber under temperatures closer to operation, *ex-situ* N_o measurements were performed on $Cs_{0.2}FA_{0.8}PbI_3$ films with a layer stack of ITO-Glass/MHP/solvent C [Figure 2 (inset)] before and after exposure to 45 and 65°C separately for 96 h in a N_2 glovebox following the transient dark current method to understand the evolution of N_o with aging. Note that in all cases, the solvent C electrode was added after each aging step to prevent interactions with the MHP layer. The films were aged with a glass substrate placed on top to simulate encapsulation/device integration without adding layers that could electrochemically interact with the MHP. This prevented the expulsion of iodine from the MHP lattice with a surface directly above the film and may explain why the

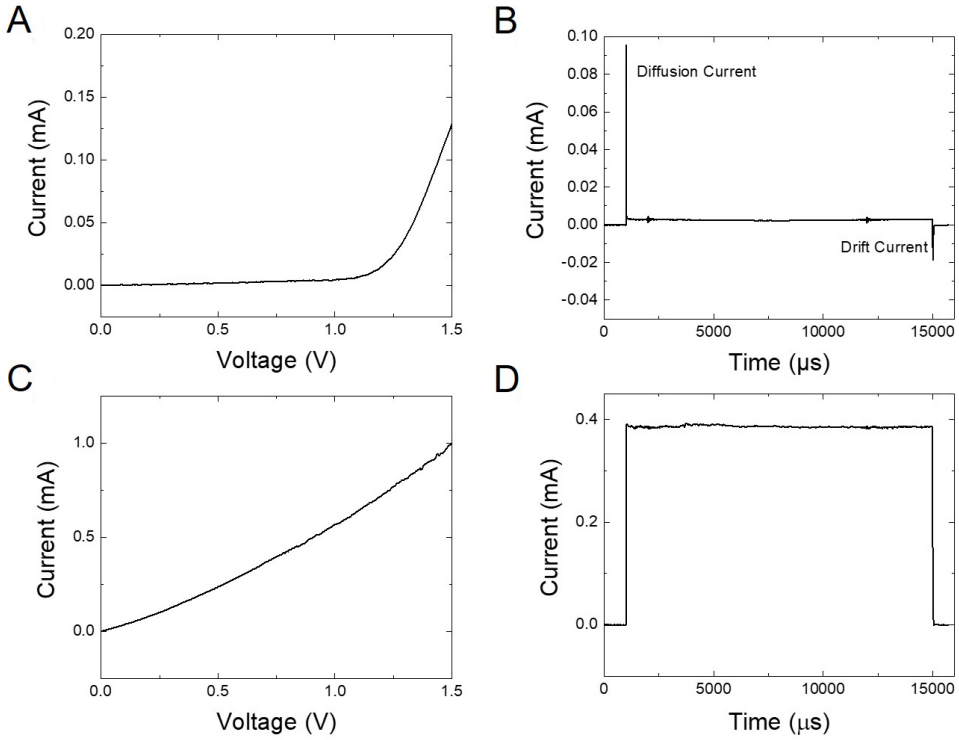

Figure 1. (A) I-V response of pristine $MAPbI_3$ films with voltage applied from 0 to 1.5 V, (B) Transient dark current response of pristine $MAPbI_3$ films. (C) I-V response after 24 h exposure at 85 °C. (D) Transient dark current response after 24 h exposure at 85 °C, where no ionic response is detectable after degradation.

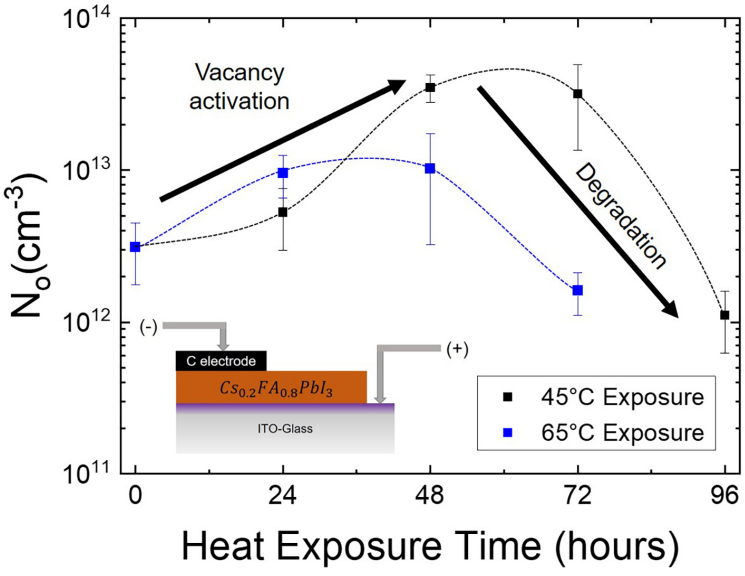

Figure 2. N_o *vs.* time of $Cs_{0.2}FA_{0.8}PbI_3$ films after exposure to heat at 45 and 65 °C with black scatter points representing exposure to 45 °C and blue scatter points representing exposure to 65 °C respectively. An initial increase in N_o is observed due to vacancy activation with exposure to heat and an eventual decrease in N_o due to degradation of $Cs_{0.2}FA_{0.8}PbI_3$ films with exposure to heat for the temperatures 45 and 65 °C, respectively. Inset - Device stack structure of $Cs_{0.2}FA_{0.8}PbI_3$ films in the form of ITO-Glass/MHP/solvent-C, with the arrows representing the contact points for probes and the signs representing polarity of the bias (forward bias).

film degraded significantly more without the additional glass substrate (as shown by the redshift in the photoluminescence peaks in Supplementary Figures 2 and 3, Supplementary Table 1).

Figure 2 shows the evolution of N_o in $Cs_{0.2}FA_{0.8}PbI_3$ films *vs.* time with aging, where the value of N_o has an initial increase after exposure to heat and then plateaus before eventually reducing in value with aging. $Cs_{0.2}FA_{0.8}PbI_3$ films did not have a N_o measurement at 96 h when subjected to 65 °C as the films did not have any electronic response after the aforementioned exposure. We hypothesize that the initial increase in the value of N_o is due to the creation of more iodide vacancies from heating and the eventual reduction is due to the degradation of the film with external stimuli leading to a loss of electronic response (corroborated by the decreased photoluminescence peaks in Supplementary Figures 4 and 5, Supplementary Table 2), which, in turn, affects the ionic measurement (as in Figure 1C) rather than an inherent reduction in the number of halide vacancies.

To understand the effect temperature has on N_o in PSCs, *in-situ* transient dark current measurements were taken as the PSCs underwent heating and cooling in a N_2 glovebox with a comparison of the highly mobile/reactive Ag electrode compared to an inert solvent-free C electrode. As shown in Figure 3, both PSCs showed a strong positive correlation with N_o *vs.* temperature with the C electrode PSC exhibiting ~10× less mobile ions than the Ag electrode PSC. At the higher temperatures, the Ag electrode PSC had approximately ~1.0×10^{15} and 1.0×10^{13} cm^{-3} mobile ions at lower temperatures while the C electrode device contained ~1.0×10^{14} and ~5.0×10^{12} cm^{-3}, respectively. The PSCs exhibit higher activation energies at lower temperatures and activation energies at higher temperatures based on the distinct slopes of N_o in Figure 3 for both Ag and C electrode PSCs where the slope of N_o *vs.* temperature is higher below 10 °C and is lower above 10 °C which is similar to the behavior of ion conductivity *vs.* temperature[43]. The C electrode PSC had a lower ion concentration dependence on temperature with less than two orders of magnitude change from higher to lower temperatures as compared to the full two orders of magnitude change in the Ag electrode PSC. This may be attributed to the inertness of the C as compared to Ag but the difference in device composition (as the C electrode device had a 2D MHP layer) may also have had an effect in this case.

To study the effect of the top electrode on N_o in the same device architecture, we performed a follow-up study where solvent-free C and Ag electrodes were deposited on different parts of identical substrates, and N_o measurements were conducted. $MAPbI_3$ PSCs were subjected to heat for 72 h in which *ex-situ*/*in-situ* dark I-V and N_o measurements were conducted. Measurements were made either *in-situ* at 65 °C while aging or *ex-situ* at room temperature after aging at 65 °C. Note that in all cases, the *in-situ* values were higher than the *ex-situ* values, an expected result due to ion activation at the higher temperature and observed in Figure 3 for both Ag and C electrodes.

There were three Ag electrodes and one C electrode on the PSC where each was measured separately depicting a more accurate comparison of the experiment as a whole. In Figure 4A, the C electrode showed a much tighter range of N_o values with the *in-situ* and *ex-situ* measurements residing within one order of magnitude of each other as compared to the wider range seen in Ag.

This contributes to the claim that Ag plays a large role in N_o at elevated temperatures due to its inherent ionic properties. The large overall increase in N_o from *ex-situ* to *in-situ* shown in Ag is hypothesized to be Ag ions becoming mobile in the PSC in conjunction with the already mobile halide ions[24]. More investigation is needed to validate this possible effect, but the results indicate a clear effect of electrode composition on N_o. The dark I-V curves in Figure 4B and C further illustrate the degradation occurring in the Ag electrode PSCs compared to the thermally stable C electrode PSCs.

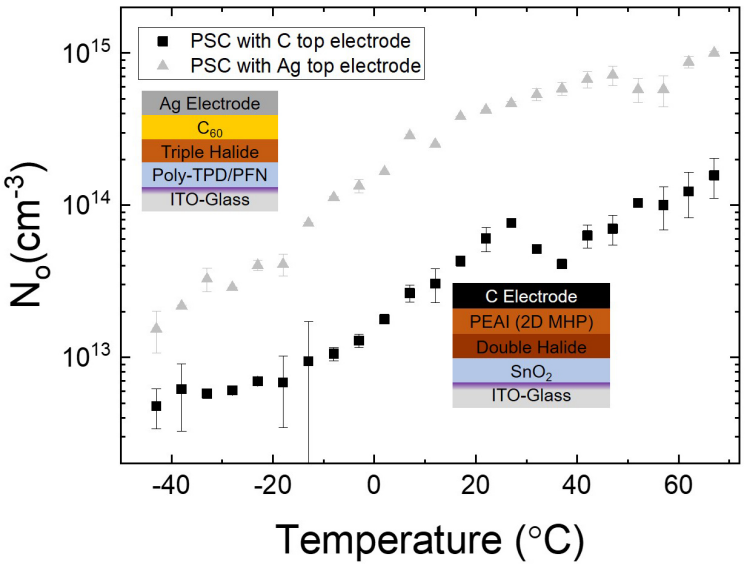

Figure 3. N_o *vs.* temperature in the range of 230 to 340 K of PSCs with an Ag top electrode and solvent-free C top electrode. The PSC with C top electrode displayed lower N_o throughout the tested temperature range when compared to PSC with Ag top electrode. Inset - Top left - Device stack structure of PSC with Ag top electrode-ITO-Glass/Poly-TPD/PFN/$Cs_{0.22}FA_{0.78}Pb(I_{0.85}Br_{0.15})_3$ + 4% $MAPbCl_3$/C_{60}/Ag, Bottom right - Device stack structure of PSC with C top electrode-ITO-Glass/SnO_2/$Cs_{0.05}FA_{0.81}MA_{0.14}PbI_{2.55}Br_{0.45}$ /PEAI(2D MHP)/solvent-free C.

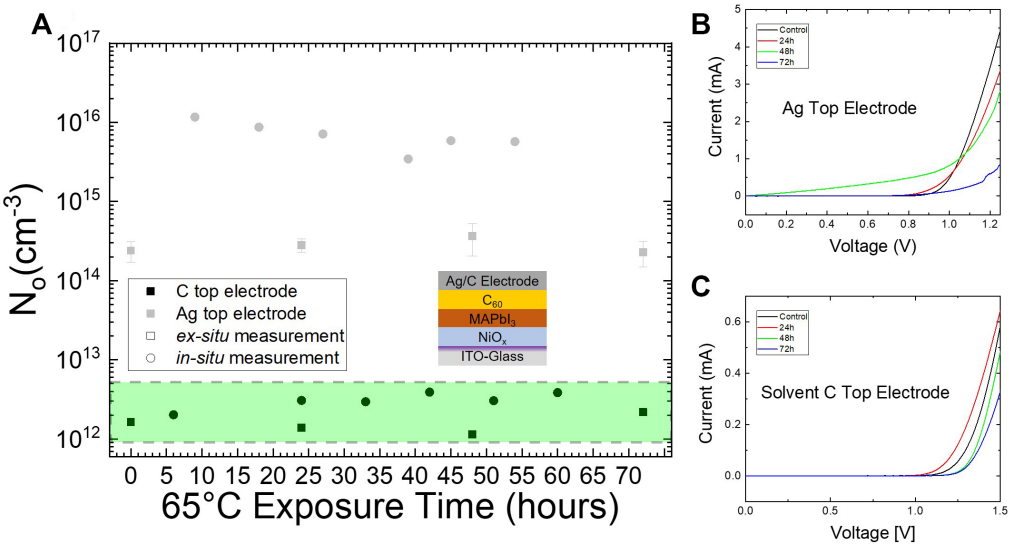

Figure 4. (A) N_o *vs.* time of PSC after exposure to 65 °C for 72 h with grey scatter points representing N_o measured from Ag top electrode and black scatter points representing N_o measured from C top electrode on the same substrate with *in-situ* and *ex-situ* measurements having circle and square shapes respectively. The C top electrode displays lower and more consistent N_o values when compared to Ag top electrode throughout the tested period. Inset - Device stack structure of PSC - ITO-Glass/NiO_x/$MAPbI_3$/C_{60}/Ag or C, both the electrodes are deposited on the same substrate. (B) I-V response *vs.* time of the PSC when measured from the Ag top electrode showing degradation with aging. (C) I-V response *vs.* time of the PSC when measured from the C top electrode showing good current response throughout the tested period.

The dark I-V curves were obtained by measuring the same electrode at each time stamp in the heat exposure process. The 48 h I-V measurement for the Ag electrode in Figure 4B shows a heavily decayed response compared to the 72 h measurement. This is possibly due to uneven degradation of the measured

Ag electrode surface causing slight variations in measurement due to probe contact location. This was not present in the C electrode where there was no variation across the surface as shown with the identically shaped I-V curves in Figure 4C. Note that when focusing on the higher voltage section of the curves (past turn-on voltage), we can see that both electrodes show a decrease in slope as aging time increases indicating an increase in series resistance across the PSC[44], an effect that is more dramatic for Ag than C [Supplementary Table 3]. In addition, Supplementary Figure 6 shows the changes in electronic and ionic properties of PSCs with Ag electrode with exposure time at 65 °C, where J_{sc} drops continually over the course of the 72 h exposure. These results show that with this $MAPbI_3$ PSC, the C electrode is more stable both ionically and electronically.

To understand the effects of N_o on other MHP properties such as mechanical durability and material composition, we hypothesized that the reduction in N_o resulting from robust bonding in the MHP would lead to fewer chemical changes in the MHP and hence could improve interfacial adhesion. G_c is a key metric of thermomechanical reliability and quantifies adhesion in thin film materials and devices. N_o measurements of the PSCs [Figure 5A and B] were performed along with G_c measurements of the PSCs by sandwiching them between glass substrates [Figure 5C] to correlate G_C with N_o. The following device stacks were used for the above measurements ITO-Glass/NiO_x/$MAPbI_3$/C60/(Ag/solvent-C/solvent-free C). These device stacks were chosen to measure and understand the variation in N_o based on the top electrode observed from our previous work[6]. From Figure 5C, the N_o with a Ag top electrode is ~6.0×10^{14} cm^{-3} and G_C is 0.8 J m^{-2}, the N_o with a solvent-free C electrode is ~2.0×10^{13} cm^{-3} and G_C is 2.8 J m^{-2}, and the N_o with a solvent C electrode is ~5.0×10^{11} cm^{-3} and G_C is 2.3 J m^{-2}. As such, PSCs with an Ag top electrode have a higher N_o and lower G_c than PSCs with a C top electrode, which has a lower N_o and higher G_c. Using C as the top electrode instead of Ag is beneficial because it suppresses ion migration and improves bonding. The main challenge limiting the usage of C electrodes in PSCs is to achieve comparable electronic conductivity to Ag[40].

Lastly, N_o measurements were performed on MHP films of different compositions to correlate mobile ions with the composition of the MHP [Figure 6 (inset)]. N_o was quantified for various compositions of 2D MHPs such as RP phase (with butylammonium) $n = 1$, $n = 2$, and DJ phase (with propane-1,3-diammonium) $n = 1$, $n = 4$[45], and 3D MHPs such as $CsPbI_3$ in addition to $MAPbI_3$. From Figure 6, N_o of the 2D MHPs is lower than the 3D MHPs, where the former ranges from ~9.0×10^9 to ~1.0×10^{11} cm^{-3}, and the latter falls between ~1.8×10^{11} and ~2.5×10^{11} cm^{-3} for the measured samples. These values of N_o across different compositions of MHPs indicate variation according to the composition. We conclude that 2D MHPs have lower N_o than the 3D MHPs, indicating that MHP dimensionality and structure also affect N_o in these materials. This could be due to the 2D MHP lattice creating more tightly bound halides due to the constraint imposed by the bulky organic cations, thus reducing the concentration of mobile halide vacancies that dominate the MHP film[14]. As shown in Figure 6, $n = 1$ 2D RP MHP exhibits a lower N_o than $n = 1$ 2D DJ MHP. Additionally, Figure 6 illustrates the slope change in N_o with increasing n-value, which is lower for 2D DJ MHP than for 2D RP MHP. We attribute this difference in behavior to the hydrogen bonding with weak Van Der Waals forces of the monoammonium cation (butylammonium) in RP phase 2D MHP and the strong hydrogen bonding of the diammonium cation (1,3-propanediammonium) between the inorganic layers which we hypothesize can more effectively prevent the activation and movement of mobile ions[46].

CONCLUSIONS

We demonstrated that our mobile ion characterization platform can quantify MHP properties in films and devices, where the dimensionality and composition of the MHP play a role on N_o. Additionally, N_o can characterize stability over time through vacancy formation and subsequent degradation. The use of C-based

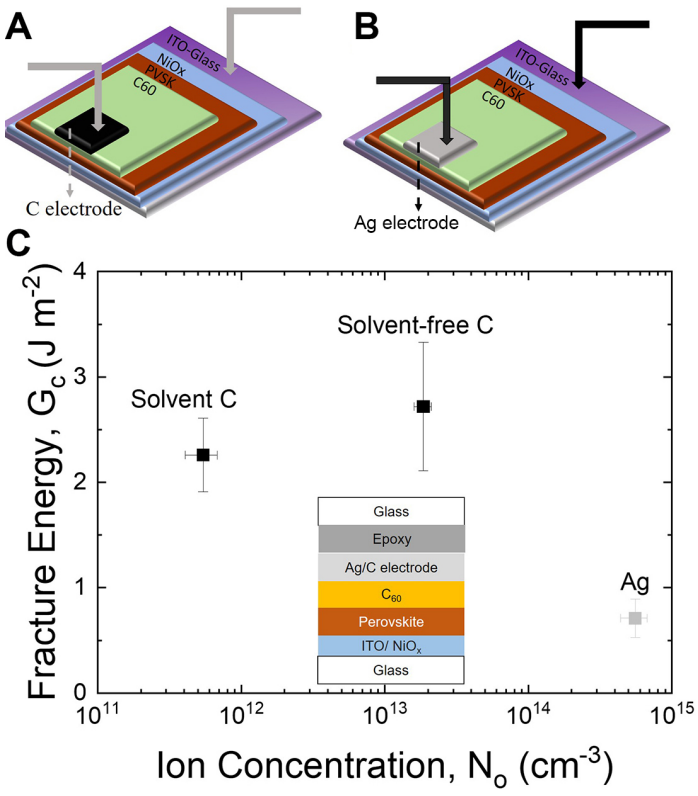

Figure 5. (A and B) Device stack structure of PSC used for N_o measurement in (C), (A) ITO-Glass/NiO_x/$MAPbI_3$/C_{60}/solvent or solvent-free C electrode, (B) ITO-Glass/NiO_x/$MAPbI_3$/C_{60}/Ag electrode, Arrows in (A and B) represent probe contact points while performing the measurement, (C) G_c *vs.* N_o of PSCs with C or Ag top electrodes showing lower N_o and higher G_c with Ag top electrode. Inset - Device stack structure (sandwich structure) used for G_c measurements - Glass/ITO/NiO_x/$MAPbI_3$/C_{60}/Ag or C electrode/epoxy/glass.

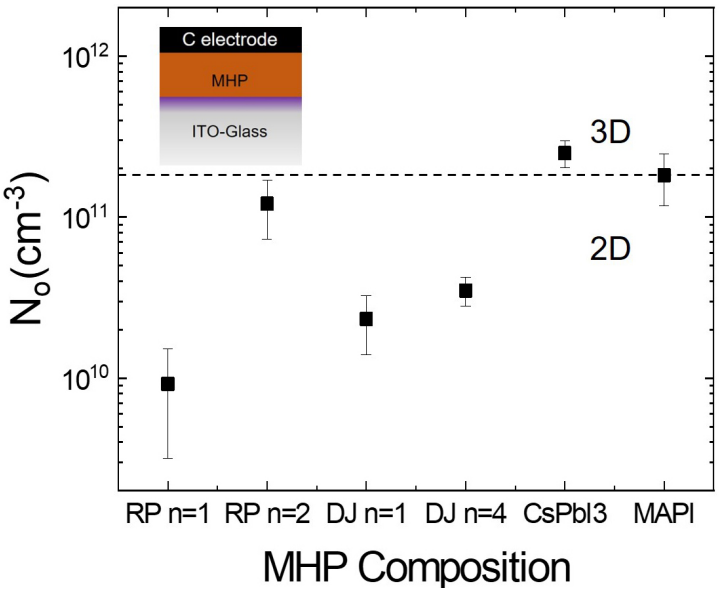

Figure 6. N_o *vs.* composition of MHP thin films with black dotted line distinguishing N_o values of 3D and 2D perovskite compositions. Inset - Device stack structure of MHP thin films in the form of ITO-Glass/MHP/solvent C.

electrodes was shown to significantly reduce N_o across a range of temperatures and device architectures while simultaneously improving the mechanical reliability of the device stack. Future work will include efforts to correlate changes in power conversion efficiency to N_o in PSCs using higher conductivity C-based electrode materials with improved band alignment to the underlying layers that facilitate higher efficiencies[47]. Although we hypothesize that halide vacancies comprise the mobile ion species, more work is necessary to determine the precise chemistry of the ions and how they change with aging.

We also speculate that the presence of metal (specifically Ag) directly contributes to the increase in N_o values. Future work will involve efforts to quantify the link more closely between N_o and stability using a larger variety of tools/methods. The fundamental understanding from this work can help inform stable device design in MHPs and PSCs.

DECLARATIONS

Acknowledgments

The authors acknowledge resources and support from the Advanced Electronics and Photonics and Solar Fabrication Lab Core Facilities at Arizona State University.

Authors' contributions

Conceptualization, visualization, methodology: Penukula S, Rolston N
Validation, formal analysis, resources, data curation, software: Penukula S, Tippin F
Investigation: Penukula S, Tippin F, Li M, Khawaja KA
Writing-original draft: Penukula S, Tippin F, Khawaja KA, Rolston N
Supervision: Penukula S, Rolston N, Yan F
Project administration, funding acquisition: Rolston N, Yan F
All authors have read and agreed to the published version of the manuscript.

Availability of data and materials

Data will be made available upon reasonable request to the corresponding author.

Financial support and sponsorship

This material is based upon work supported by the U.S. Department of Energy's Office of Energy Efficiency and Renewable Energy (EERE) under Solar Energy Technologies Office (SETO) Agreement Number DE-EE0011152. This work is supported by the National Science Foundation Under Grant No. TI-2329871 "Highly Efficient, Scalable, and Stable Carbon-based Perovskite Solar Modules".

Conflicts of interest

All authors declared that there are no conflicts of interest.

Ethical approval and consent to participate

Not applicable.

Consent for publication

Not applicable.

Copyright

© The Author(s) 2024.

REFERENCES

1. NREL. Champion photovoltaic module efficiency chart. Available from: https://www.nrel.gov/pv/module-efficiency.html [Last accessed on 5 Jun 2024].
2. Bhattacharya S, John S. Beyond 30% conversion efficiency in silicon solar cells: a numerical demonstration. *Sci Rep* 2019;9:12482. DOI PubMed PMC
3. Čulík P, Brooks K, Momblona C, et al. Design and cost analysis of 100 MW perovskite solar panel manufacturing process in different locations. *ACS Energy Lett* 2022;7:3039-44. DOI
4. NREL. Best research-cell efficiency chart. Available from: https://www.nrel.gov/pv/cell-efficiency.html [Last accessed on 5 Jun 2024].
5. Rivkin B, Fassl P, Sun Q, Taylor AD, Chen Z, Vaynzof Y. Effect of ion migration-induced electrode degradation on the operational stability of perovskite solar cells. *ACS Omega* 2018;3:10042-7. DOI PubMed PMC
6. Penukula S, Estrada Torrejon R, Rolston N. Quantifying and reducing ion migration in metal halide perovskites through control of mobile ions. *Molecules* 2023;28:5026. DOI PubMed PMC
7. Bi E, Song Z, Li C, Wu Z, Yan Y. Mitigating ion migration in perovskite solar cells. *Trends Chem* 2021;3:575-88. DOI
8. Tayagaki T, Yamamoto K, Murakami TN, Yoshita M. Temperature-dependent ion migration and mobile-ion-induced degradation of perovskite solar cells under illumination. *Solar Energy Mater Solar Cells* 2023;257:112387. DOI
9. Wu Z, Yuan S, Miao S, et al. Unraveling the rapid ion migration in perovskite solar cells by circuit-switched transient photoelectric technique. *J Chem Phys* 2024;160:111101. DOI
10. Zai H, Ma Y, Chen Q, Zhou H. Ion migration in halide perovskite solar cells: mechanism, characterization, impact and suppression. *J Energy Chem* 2021;63:528-49. DOI
11. Zhao Y, Zhou W, Han Z, Yu D, Zhao Q. Effects of ion migration and improvement strategies for the operational stability of perovskite solar cells. *Phys Chem Chem Phys* 2021;23:94-106. DOI
12. Liu J, Hu M, Dai Z, Que W, Padture NP, Zhou Y. Correlations between electrochemical ion migration and anomalous device behaviors in perovskite solar cells. *ACS Energy Lett* 2021;6:1003-14. DOI
13. Hossain MI, Tong Y, Shetty A, Mansour S. Probing the degradation pathways in perovskite solar cells. *Solar Energy* 2023;265:112128. DOI
14. Mathew P, Cho J, Kamat PV. Ramifications of ion migration in 2D lead halide perovskites. *ACS Energy Lett* 2024;9:1103-14. DOI
15. Huang Z, Proppe AH, Tan H, et al. Suppressed ion migration in reduced-dimensional perovskites improves operating stability. *ACS Energy Lett* 2019;4:1521-7. DOI
16. Grancini G, Nazeeruddin MK. Dimensional tailoring of hybrid perovskites for photovoltaics. *Nat Rev Mater* 2019;4:4-22. DOI
17. Zhao X, Liu T, Loo YL. Advancing 2D perovskites for efficient and stable solar cells: challenges and opportunities. *Adv Mater* 2022;34:e2105849. DOI
18. Ortiz-Cervantes C, Carmona-Monroy P, Solis-Ibarra D. Two-dimensional halide perovskites in solar cells: 2D or not 2D? *ChemSusChem* 2019;12:1560-75. DOI
19. Ma K, Sun J, Atapattu HR, et al. Holistic energy landscape management in 2D/3D heterojunction via molecular engineering for efficient perovskite solar cells. *Sci Adv* 2023;9:eadg0032. DOI PubMed PMC
20. Zouhair S, Clegg C, Valitova I, March S, Jailani JM, Pecunia V. Carbon electrodes for perovskite photovoltaics: interfacial properties, meta-analysis, and prospects. *Solar RRL* 2024;8:2300929. DOI
21. Besleaga C, Abramiuc LE, Stancu V, et al. Iodine migration and degradation of perovskite solar cells enhanced by metallic electrodes. *J Phys Chem Lett* 2016;7:5168-75. DOI
22. Domanski K, Correa-Baena JP, Mine N, et al. Not all that glitters is gold: metal-migration-induced degradation in perovskite solar cells. *ACS Nano* 2016;10:6306-14. DOI
23. Parashar M, Sharma M, Saini DK, et al. Probing elemental diffusion and radiation tolerance of perovskite solar cells via non-destructive Rutherford backscattering spectrometry. *APL Energy* 2024;2:016109. DOI
24. Kerner RA, Cohen AV, Xu Z, et al. Electrochemical doping of halide perovskites by noble metal interstitial cations. *Adv Mater* 2023;35:e2302206. DOI
25. Sun X, Lin T, Ding C, et al. Fabrication of opaque aluminum electrode-based perovskite solar cells enabled by the interface optimization. *Org Electron* 2022;104:106475. DOI
26. Svanström S, García-Fernández A, Jacobsson TJ, et al. The complex degradation mechanism of copper electrodes on lead halide perovskites. *ACS Mater Au* 2022;2:301-12. DOI PubMed PMC
27. Chen H, Yang S. Stabilizing and scaling up carbon-based perovskite solar cells. *J Mater Res* 2017;32:3011-20. DOI
28. Hadadian M, Smått J, Correa-baena J. The role of carbon-based materials in enhancing the stability of perovskite solar cells. *Energy Environ Sci* 2020;13:1377-407. DOI
29. Baghestani E, Tajabadi F, Saki Z, et al. A conductive adhesive ink for carbon-laminated perovskite solar cells with enhanced stability and high efficiency. *Solar Energy* 2023;266:112165. DOI
30. Zhu A, Chen L, Zhang A, et al. Playdough-like carbon electrode: a promising strategy for high efficiency perovskite solar cells and modules. *eScience* 2024;4:100221. DOI
31. Jeon I, Seo S, Sato Y, et al. Perovskite solar cells using carbon nanotubes both as cathode and as anode. *J Phys Chem C*

2017;121:25743-9. DOI

32. Zhang J, Hu XG, Ji K, et al. High-performance bifacial perovskite solar cells enabled by single-walled carbon nanotubes. *Nat Commun* 2024;15:2245. DOI PubMed PMC
33. Zhang C, Wang S, Zhang H, et al. Efficient stable graphene-based perovskite solar cells with high flexibility in device assembling *via* modular architecture design. *Energy Environ Sci* 2019;12:3585-94. DOI
34. Gan Y, Sun J, Guo P, et al. Advances in the research of carbon electrodes for perovskite solar cells. *Dalton Trans* 2023;52:16558-77. DOI
35. Pandey S, Karakoti M, Bhardwaj D, et al. Recent advances in carbon-based materials for high-performance perovskite solar cells: gaps, challenges and fulfillment. *Nanoscale Adv* 2023;5:1492-526. DOI PubMed PMC
36. Fagiolari L, Bella F. Carbon-based materials for stable, cheaper and large-scale processable perovskite solar cells. *Energy Environ Sci* 2019;12:3437-72. DOI
37. Yu Y, Hoang MT, Yang Y, Wang H. Critical assessment of carbon pastes for carbon electrode-based perovskite solar cells. *Carbon* 2023;205:270-93. DOI
38. Nguyen H, Penukula S, Mahaffey M, Rolston N. All inorganic $CsPbI_3$ perovskite solar cells with reduced mobile ion concentration and film stress. *MRS Commun* 2024;14:208-14. DOI
39. Xu J, Boyd CC, Yu ZJ, et al. Triple-halide wide-band gap perovskites with suppressed phase segregation for efficient tandems. *Science* 2020;367:1097-104. DOI
40. Vijayaraghavan SN, Wall J, Xiang W, et al. Carbon electrode with sputtered Au coating for efficient and stable perovskite solar cells. *ACS Appl Mater Interfaces* 2023;15:15290-7. DOI
41. Zhang H, Xiao J, Shi J, et al. Self-adhesive macroporous carbon electrodes for efficient and stable perovskite solar cells. *Adv Funct Mater* 2018;28:1802985. DOI
42. Li M, Johnson S, Gil-escrig L, et al. Strategies to improve the mechanical robustness of metal halide perovskite solar cells. *Energy Adv* 2024;3:273-80. DOI
43. Han B, Yuan S, Cai B, et al. Green perovskite light-emitting diodes with 200 hours stability and 16% efficiency: cross-linking strategy and mechanism. *Adv Funct Mater* 2021;31:2011003. DOI
44. Morales-aragonés JI, Alonso-garcía MDC, Gallardo-saavedra S, et al. Online distributed measurement of dark I-V curves in photovoltaic plants. *Appl Sci* 2021;11:1924. DOI
45. Liu R, Hu X, Xu M, Ren H, Yu H. Layered low-dimensional ruddlesden-popper and dion-jacobson perovskites: from material properties to photovoltaic device performance. *ChemSusChem* 2023;16:e202300736. DOI
46. Ahmad S, Fu P, Yu S, et al. Dion-jacobson phase 2D layered perovskites for solar cells with ultrahigh stability. *Joule* 2019;3:794-806. DOI
47. Chen K, Xiao X, Liu J, et al. Record-efficiency printable hole-conductor-free mesoscopic perovskite solar cells enabled by the multifunctional schiff base derivative. *Adv Mater* 2024;36:e2401319. DOI